Int. J. Electrochem. Sci., 15 **(2020)** 7228 – 7241, doi: 10.20964/2020.08.65

International Journal of
ELECTROCHEMICAL
SCIENCE
www.electrochemsci.org

Corrosion assessment of Ag and Cr modified Fe40Al intermetallic alloy in Hank´s solution by electrochemical noise

R. A. Rodriguez-Diaz[1,*], *J. L. Reyes-Barragán*[2], *C.D. Arrieta-Gonzalez*[3], *J. Porcayo-Calderon*[4], *S. Serna*[4,]

[1] Academy-Industry Coperation Center CCAI, Technologic of Superior Studies of Coacalco, Coacalco de Berriozabal, Edo de México, 55700, México.
[2] Polytechnic University of Metropolitan Zone of Guadalajara, Tlajomulco de Zúñiga, Jalisco 45640, Mexico.
[3] National Technologic of México – Technologic Institute of Zacatepec, Calzada Instituto Tecnológico 27, 62780 Zacatepec, MOR, México
[4] Research Center in Engineering and Applied Sciences - UAEM, Av. Universidad 1001, Chamilpa 62209, Cuernavaca Morelos, México.
[*]E-mail: german.rodericus@gmail.com

Received: 2 Seprember 2019 / *Accepted:* 28 January 2020 / *Published:* 10 July 2020

This research presents an evaluation of the corrosion performance of binary Fe40Al alloy and ternary Fe40Al-2.5Cr and Fe40Al-2.5Ag (at %) alloys exposed to a synthetic physiological solution that simulates biological human body fluids. Electrochemical noise measurements were made on Fe40Al based alloys during exposure to the biomimetic solution over a 30-day period. The electrochemical parameters of the evaluated alloys were compared. Polarization curves revealed that the corrosion current density of the Cr-modified Fe40Al alloy was less than that of the ternary Fe40Al-2.5Ag alloy; regarding electrochemical noise measurements, analyses revealed that both ternary alloys experienced a pitting corrosion during the entire immersion period. Additionally, the alloy Fe40Al-2.5Cr predominantly exhibited a higher corrosion rate than the Ag-modified intermetallic for the entire exposure time.

Keywords: Iron aluminides, corrosion, electrochemical noise, microstructural characterization, Hank´s solution

1. INTRODUCTION

For decades, various materials have been commonly used to replace or repair a tissue, body characteristic, or function in various areas of medical sciences including biomedical engineering and dentistry. The proper functioning of biomaterials that contact living tissue is determined by biocompatibility and biofunctionality.

One aspect that greatly influences the biocompatibility of metallic biomaterials is corrosion resistance and the corrosion products that are liberated onto the surrounding tissue [1]. For example, the corrosion products of dental alloys possess metal ions which may induce allergic reactions and some diseases. For this reason, the electrochemical behavior of non-precious alloys has been the subject of various investigations [2].

The corrosion resistance of the most commonly used metallic materials, including austenitic stainless steels, Co-Cr alloys, Ti and Ti-based implant alloys, is determined by their passivation nature, which is controlled by a thin oxide surface layer [3-6].

The ideal properties for metallic biomaterials are as follows: biocompatible chemical composition to evade harmful tissue reactions, excellent resistance to degradation or corrosion, appropriate strength to maintain cyclic loading supported by the joint, elevated modulus to decrease the bone resorption, and high wear resistance to minimize wear waste generation [7].

Physiological media are naturally extremely adverse and unfavorable to any external materials; therefore, the effect of the environment on the metallic implants and the influence of the metallic implant on its host tissue are main subjects of concern. Notably, the physiological environment has an elevated concentration of chloride ions, representing a highly corrosive medium for metallic implants [8].

Intermetallic compounds, such as transition metal aluminides, have orderly crystalline structures and good structural performance. Their Al content promotes the formation of a protective layer (Al_2O_3) with good resistance to oxidation, corrosion and sulfurization at and above room temperature. Additionally, these intermetallic compounds maintain good strength [9-12].

Over the last few decades, corrosion behavior of aluminides has been increasingly investigated due to their excellent performance in aqueous media including acidic, basic, chloride-rich and sulfur compound solutions. For these reasons, iron aluminides are among the materials considered for metallic biomaterial substitutes [13-15].

Hence, the object of this research is to assess the corrosion behavior of Fe40Al, with additions of Ag and Cr by means of electrochemical techniques, when the intermetallic compounds are exposed to Hank´s solution for a short period of time.

2. EXPERIMENTAL PROCEDURE

2.1. Materials

The intermetallic alloys evaluated (Fe40Al, Fe40Al-2.5Ag, Fe40Al-2.5Cr, at %) were manufactured in an induction furnace. High purity elements (99.9%) were used in all cases. Stoichiometric amounts of each element were placed inside a SiC crucible for induction melting. The molten alloys were poured into steel molds and allowed to cool to room temperature. The ingots produced exhibited coarse-grained microstructures.

2.2. Hank's Solution

The intermetallic alloys were exposed to a biomimetic solution (Hank's solution). The composition of the corrosive medium was: 8.0 g/L NaCl, 0.4 g/L KCl, 0.06 g/L KH_2PO_4, 1.0 g/L glucose

($C_6H_6O_6$), 0.048 g/L Na_2HPO_4, 0.098 g/L $MgSO_4 \cdot 7H_2O$, 0.14 g/L $CaCl_2$ and 0.35 g/L $NaHCO_3$ using distilled water. The solution had pH 7.2 and was prepared with analytical grade chemical reagents.

2.3. Corrosion Tests

Corrosion tests were carried out at 36.5 °C with 200 ml of Hank's solution. The specimens were prepared by sequential grinding with SiC paper up to #2000 finishing and then polished with a suspension of 1.0 micron alumina particles. Finally, they were washed with water and degreased with acetone.

A computer-controlled potentiostat was used to generate the potentiodynamic polarization curves. These were obtained at a 1 mV/s scanning rate using a three electrode electrochemical cell. A saturated Ag/AgCl electrode was used as a reference electrode and a graphite rod was used as a counter electrode. The polarization range was -1000 mV to 1000 mV with respect to the corrosion potential of the working electrode.

Electrochemical noise measurements, EN (potential and current), were obtained using an electrochemical cell similar to that used for potentiodynamic polarization curves. Fluctuations of current and potential were obtained at a sampling rate of 1 point per second for 1024 seconds using a zero resistance ammeter (ZRA) (ACM Instruments). The obtained signals were then pre-processed by eliminating the DC trend from the raw data using the least squares adjustment method. The EN tests were conducted for 30 days.

2.4. Microstructural characterization

Specimens in as-cast conditions were analyzed by scanning electron microscopy (SEM) to reveal the microstructure. Samples were subjected to chemical microanalysis in order to determine the chemical composition of the intermetallic alloys and X-ray chemical maps were also developed for the purpose of revealing the distribution of phases and elements in all sample surfaces. For this purpose, an energy dispersive X-ray analyzer (EDX) attached to the SEM was used.

Determination of the crystal structure and identification of phases were accomplished using the X-ray diffraction technique and a Cu tube (Kα line radiation: $\lambda = 0.15406$ nm) was used for the microstructure analysis. The XRD profiles were recorded from 10-100° in the 2Θ range (step size 0.02°, time per step 0.6 s).

3. RESULTS AND DISCUSSION

3.1. Microstructural analysis

Figure 1 shows the microstructures of intermetallic alloys. Figure 1i shows the dendritic type microstructure of the Fe40Al alloy. Figure 1a displays a scanning electron micrograph of the Fe40Al-2.5Cr alloy showing columnar grain morphology with an average size of 430 µm width and 1,100 µm long. SEM and EDS analyses of the Fe40Al-2.5Cr alloy did not show precipitates caused by Cr addition.

Furthermore, element mappings corresponding to Fe40Al-2.5Cr displayed in Figures 1b, c and d reveal that the Cr is uniformly distributed into Fe40Al matrix. These findings agree with Rodriguez Diaz et al. [16-17], who reported that low concentrations of Cr (<5 at %) added to FeAl alloy induces solid solution formation. Figure 1e shows the microstructure of ternary Fe40Al-2.5Ag alloy. This secondary electron micrograph shows light gray precipitates dispersed uniformly inside various grains of the Fe40Al matrix alloy. According to point chemical analyses, X-ray diffraction and chemical mappings, these precipitates correspond to pure Ag. Furthermore, the element mappings presented in Figures 1f, g and h reveal that Ag precipitates were uniformly dispersed in the binary aluminide matrix.

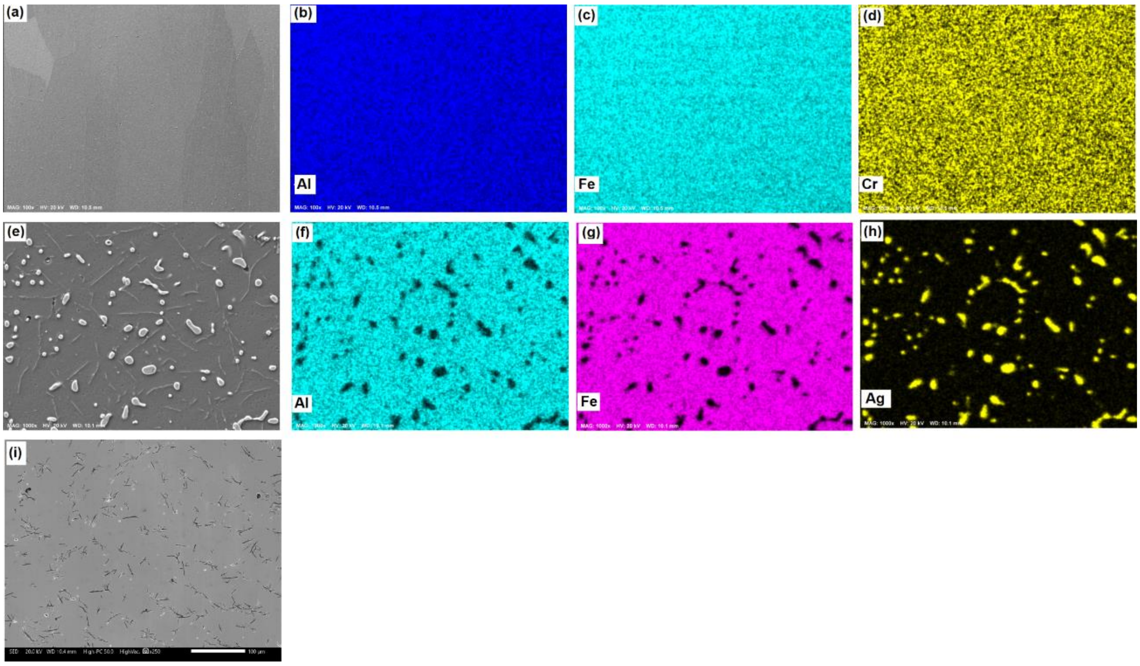

Figure 1. Scanning electron micrographs of as-cast (a) Fe40Al-2.5Cr, (e) Fe40Al-2.5Ag, and (i) Fe40Al. Element mappings of Fe40Al-2.5Cr; (b) Al, (c) Fe, (d) Cr. Element mappings of Fe40Al-2.5Ag; (f) Al, (g) Fe and (h) Ag.

Figure 2 displays the X-ray diffraction spectra of the binary Fe40Al alloy along with as-cast ternary Fe40Al-2.5X (at. %) (X = Cr and Ag) alloys. This diffractogram indicates that the ternary alloys exhibited from 2 to 4 diffraction peaks within the studied 2ϴ range. The binary Fe40Al alloy exhibited (100), (110) and (211) diffraction peaks, indicating a B2 type of crystalline structure. The absence of diffraction peaks in X-ray profiles of ternary alloys corresponds to a coarse grain size in the order of a few hundred microns to millimeters. When these kinds of intermetallics are elaborated through conventional melting and casting processes, the resultant microstructure consists mainly of coarse grains. The indexation of all diffraction patterns revealed an ordered B2 type crystalline structure that corresponds with the FeAl phase. This finding indicates that the addition of Cr did not induce modification of the crystal structure of the binary intermetallic alloy. Additionally, variation in intensity of the (111) diffraction peak, corresponding to the binary Fe40Al intermetallic alloy, is associated with a preferred crystallographic orientation. Adding Cr into the Fe40Al alloy clearly shows that the Cr element formed a solid solution in the binary matrix. The chromium solubilization process in the intermetallic matrix can be corroborated by Figure 1e, which shows the Cr element mapping; furthermore, this phenomenon is confirmed by the absence of diffraction peaks, unlike the binary intermetallic phase (see Figure 2b). This finding agrees with the ternary alloy phase diagram of the system Fe-Al-Cr [18].

The X-ray diffraction spectrum of the Fe40Al-2.5Ag alloy shows peaks belonging to both the Ag phase (FCC type crystalline structure) and the FeAl phase (B2 ordered crystalline structure), as shown in Figure 2c. This reveals that silver did not form a solid solution with the FeAl matrix. Instead, it precipitated uniformly into an aluminide matrix, as shown in Figure 1e. This is due to the immiscibility of Ag in both Fe and Al according to the corresponding phase diagrams (Fe-Ag and Fe-Al) [19, 20].

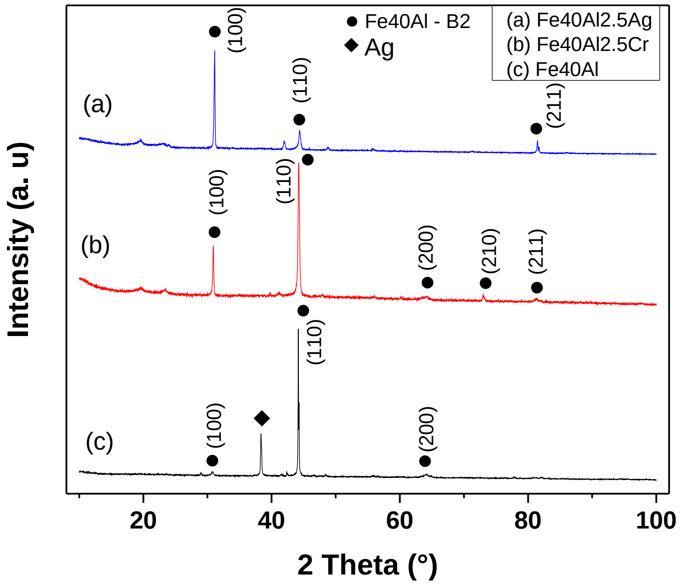

Figure 2. X-ray diffraction profiles of the Fe40Al-X alloys.

3.2. Polarization Curves

Figure 3 displays the polarization curves of binary and ternary Fe40Al alloys exposed to the synthetic physiological solution. The plot shows that the addition of Cr resulted in a noble potential, while the addition of Ag shifted the rest potential towards the active side. Similarly, Table 1 shows that the Fe40Al-2.5Cr ternary alloy had the lowest corrosion rate (corrosion current density), while the silver-added alloy had the highest values. It is notable that the addition of both Ag and Cr induced a passivation process in the binary Fe40Al surface; however, the Fe40Al-2.5Cr ternary alloy showed a more pronounced passivation phenomenon, as the Cr addition generated a re-passivation process. The Fe40Al-2.5Cr alloy exhibited a passivation process at a -247 mV potential and a re-passivation process at a -95 mV potential. The potentiodynamic polarization curves of the ternary alloys revealed pitting corrosion processes after passivation. Corrosion potentials (E_{corr}) were obtained using the saturated Ag/AgCl reference electrode and were then converted to values equivalent to the SCE reference electrode to facilitate comparison with the results of previous studies.

Castañeda et al. [21] performed potentiodynamic polarization tests on 50Ni25Al25Cu and 50Ni30Al-20Cu (wt. at %) alloys exposed to Hank's solution. The authors reported corrosion current densities of 2.75 x 10^{-5} and 6.94 x 10^{-4} mA/cm^2 for each alloy, respectively. In this case, the I_{corr} value (corrosion current density) of 50Ni30Al-20Cu is more or less equal to that of the Fe40Al alloy reported here, but higher than the corrosion current density of the Fe40Al-2.5Cr alloy. This behavior is caused by the protective nature of the Al_2O_3 layer that forms on the surface of iron aluminides. Additionally, it is apparent that the Cr addition improved the corrosion resistance of the alloy, making possible the formation of a passive layer of Al_2O_3 modified with Cr with improved passivation properties. Furthermore, a previous study of the oxidation behavior of Fe and Ni aluminides by X-ray photoelectron spectroscopy reported that Al_2O_3 is formed onto surface alloys when they are oxidized at pressures ranging from 1.3 x 10^{-6} to 1.3 Pa, whereas $NiAl_2O_4$ was formed on a clean Ni_3Al surface [22].

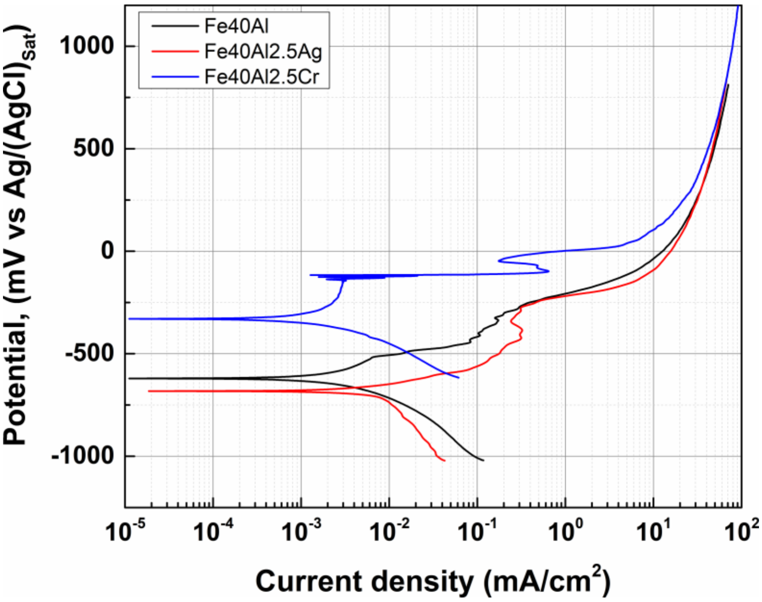

Figure 3. Polarization curves for Fe40Al, Fe40Al-2.5Cr and Fe40Al-2.5Ag alloys exposed to Hank's solution

Arrieta-Gonzalez et al. [23] performed potentiodynamic polarization testing on Ti, 316L stainless steel, Fe_3Al and Fe_3Al modified with Ni. The authors reported corrosion current densities of 4.5 x 10^{-3} and 7 x 10^{-5} mA/cm^2 for Ti and 316L respectively. The above indicates that the Al-oxide that developed on the surface of ternary intermetallic alloys under study was more protective than the Ti-oxide film formed on the commercially available Ti. Previous research has investigated the protective film formed onto Ti, e.g. M. Pisarek et al. [24] studied the surface film developed on Ti using auger electron spectroscopy (AES) and X-ray photoelectron spectroscopy (XPS). In this research, AES analyses revealed the formation of TiO_2 on the Ti surface, and XPS confirmed the AES results [24]. Conradi et al. [25] performed surface analyses on 316L stainless steel exposed to synthetic body solutions. In this research, XPS results revealed that the oxide film formed on the 316L steel surface contained Fe and Cr oxides. In this case, however, the Ni and Mo oxides were scarce compared to the bulk. Thus, the oxide mixture formed on 316L is naturally more protective than the Al-oxide film formed on binary Fe40Al and ternary FeAl-2.5Ag, FeAl-2.5Cr alloys.

Table 1. Electrochemical parameters of Fe40Al-X intermetallic alloys.

Alloy	**E_{corr} (mV)**	**B_a (mV/Dec)**	**B_c (mV/Dec)**	**I_{corr} (mA/cm^2)**
Fe40Al	-621	509	334	0.00736
Fe40Al-2.5Ag	-682	128	627	0.0108
Fe40Al-2.5Cr	-328	960	240	0.001218

3.4. Electrochemical Noise

Various electrochemical current tests were performed to evaluate the susceptibility of Fe40Al-2.5Cr and Fe40Al-2.5Ag alloys to any kind of localized corrosion at discrete sites where the protective passive layer has broken down, such as galvanic, pitting, exfoliation or intergranular attack [26-29]. Examples of the EN time series in current for the binary and ternary alloys exposed to Hank´s solution are presented in Figures 4, 5 and 6.

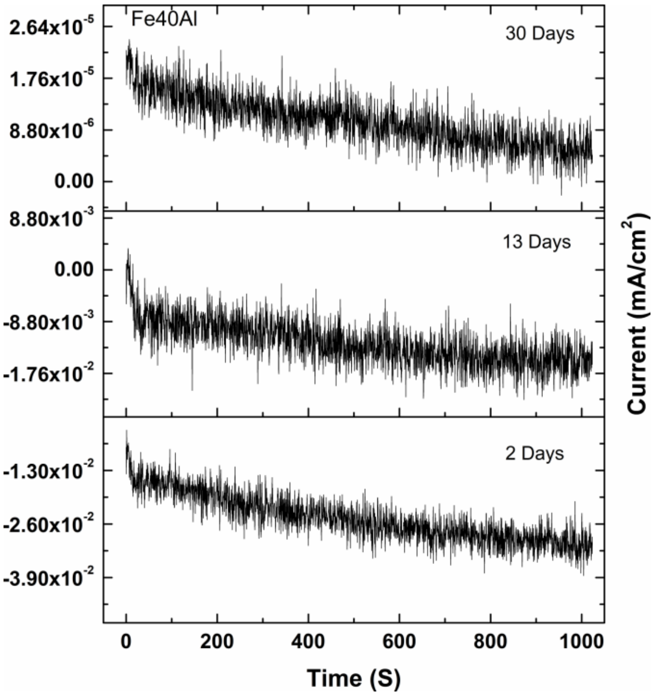

Figure 4. Electrochemical noise for Fe40Al alloy during 2, 13 and 30 immersion days in Hank's solution.

Figure 4 shows the noise current for the binary Fe40Al intermetallic alloy. In this case, large transients were present following 2, 13 and 30 days of exposure. The transient behavior observed in the current noise time series has been associated with the propagation of localized attack [30].

Figure 5 shows the noise current for Fe40Al-2.5Cr. It is apparent from the figure that at the beginning of exposure time (2 days), the current series displayed a scarce number of anodic and cathodic transients (from 750 s), showing low frequency and moderate intensity. The frequency of transients increased with immersion time, suggesting that the protective film experienced localized corrosion during and after the second day of immersion, despite the fact that the Fe40Al-2.5Cr ternary alloy was protected by the Al-oxide based layer. However, the susceptibility to localized attack increased at 13 and 30 days of exposure. Therefore, these transients are associated with breaking and reforming events of the Al-based protective film, such as localized attack initiation [31-33].

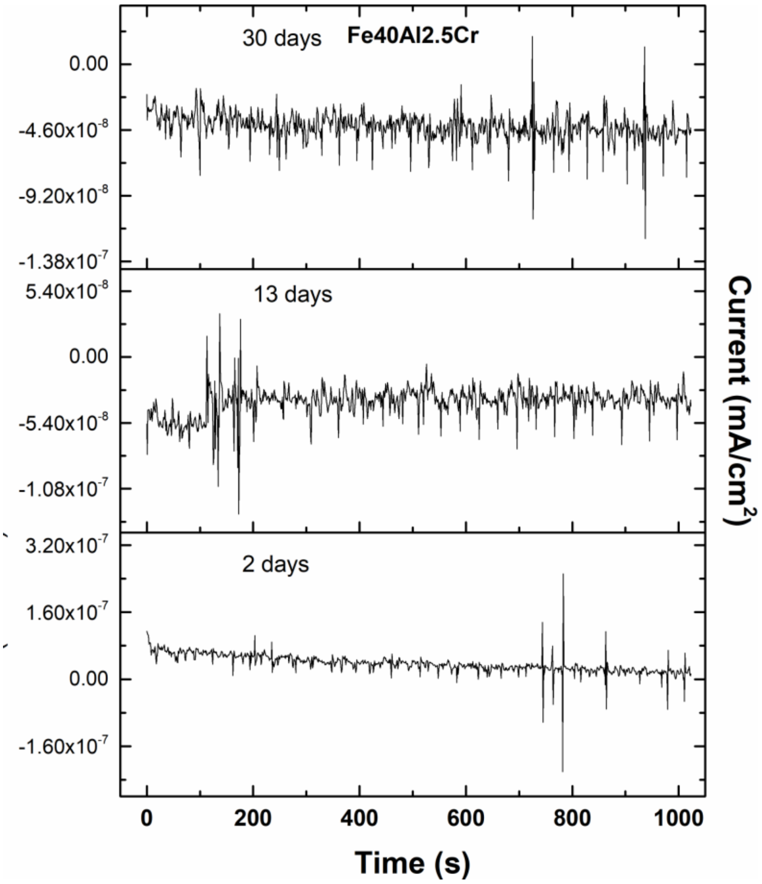

Figure 5. Electrochemical noise of Fe40Al-2.5Cr alloy after 2, 13 and 30 days of immersion in Hank solution.

Similarly, Figure 6 displays the noise current for Fe40Al-2.5Ag alloy. The graph shows that at the beginning of exposure time, the current series revealed a few anodic and cathodic transients at the second day of exposure (starting at 200 s), indicating low frequency and moderate intensity of transients. However, the frequency and intensity of transients increased with length of immersion, suggesting that the Al-based protective film on the Fe40Al-2.5Ag ternary alloy had begun to experience localized corrosion. It is apparent, however, that the susceptibility to localized attack increased at 13 and 30 days of immersion. This tendency indicates development of localized corrosion by the intermetallic alloy, which is probably due to galvanic effects in the Fe40Al matrix with pure silver. Therefore, any protective film developed on the surface is broken down, and the underlying bare alloy can be locally corroded in discrete sites. These transients are therefore associated with rupture and reforming events of the Al-oxide film, such as localized attack initiation.

The following analysis was performed on the electrochemical noise data to determine the susceptibility of the Fe40Al-based alloys to any type of localized corrosion, such as pitting. The noise resistance, R_n, was determined using Equation 1:

$$R_n = \frac{\sigma v}{\sigma i} \qquad 1$$

Where R_n is the noise resistance, σ_v is the standard deviation of the noise potential, and σ_i is the standard deviation of the noise current [34]. Figure 7 displays the variation of noise resistance as a function of exposure time for the intermetallic alloys. The figure shows that the Fe40Al alloy had the lowest R_n value, while the ternary Fe40Al-2.5Cr alloy had the highest R_n value. This behavior is congruent with the lowest value of corrosion current density determined for this alloy, as shown in Figure 3 and Table 1.

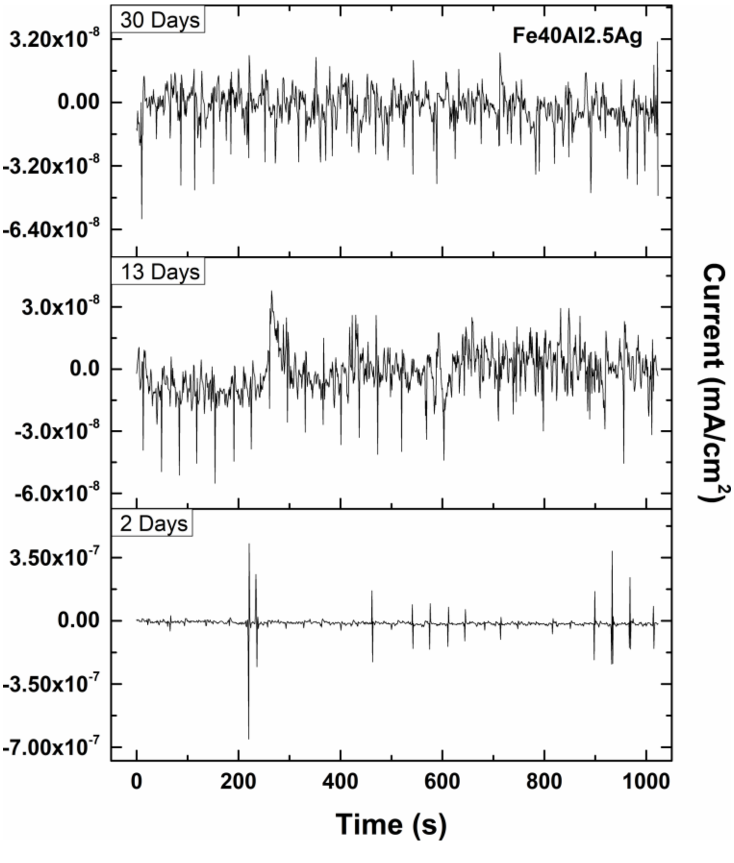

Figure 6. Electrochemical noise for Fe40Al-2.5Ag alloy after 2, 13 and 30 immersion days in Hank's solution.

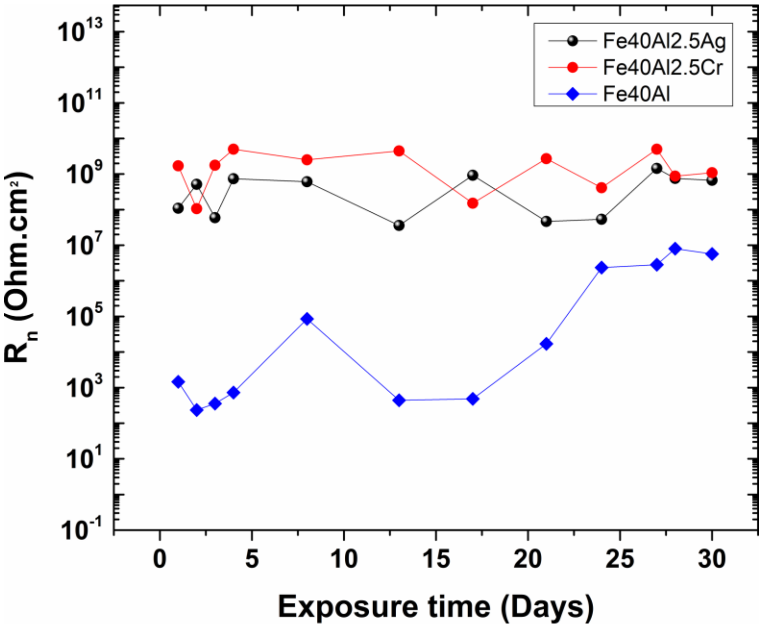

Figure 7. Variation of the noise resistance, R_n, of intermetallic alloys as a function of the immersion time in Hank's physiological solution.

Since previous papers have argued that R_n is equivalent to R_p [35-36], it can be inferred from the Stern-Geary equation [37] that binary aluminide exhibited the highest corrosion rate over the entire immersion period, while Fe40Al-2.5Cr had the lowest corrosion rate over the entire exposure time. The fact that the Fe40Al-2.5Cr alloy has the highest corrosion resistance is due to the fact that this alloy showed a greater tendency to passivation as observed in the polarization curve tests.

The localization index (LI) [35-36], or pitting damage index, is defined by:

$$LI = \frac{\sigma_i}{i_{rms}} \qquad (2)$$

In the equation, σ_i is the standard deviation of the noise current and i_{rms} is the root mean squared of the current noise. The obtained LI values represent the type of corrosion suffered by intermetallic alloys. LI values between 0.01 and 0.001 indicate a uniform corrosion process on the alloy surface. LI values between 0.1 and 0.01, however, indicate that the alloy is susceptible to both uniform and pitting corrosion. Finally, LI values between 1 and 0.1 indicate that the alloy is highly prone to pitting corrosion [38]. Table 2 displays the LI values of the intermetallic alloys in contact with Hank´s solution over a 30 day immersion period. It can be inferred that Fe40Al-2.5Cr and Fe40Al-2.5Ag alloys were prone to pitting corrosion throughout the immersion period. These findings agree with the results obtained from the polarization curves (Figure 3), where pitting processes were observed after the formation of a passive layer.

Table 2. Pitting damage index (LI) as a function of immersion time for intermetallic alloys in Hank´s solution.

Alloy	Exposure time (days)	LI	Corrosion type
Fe40Al	2	0.03	Mixed
	13	0.03	Mixed
	30	0.001	Uniform
Fe40Al-2.5Cr	2	0.51	Pitting
	13	0.31	Pitting
	30	0.22	Pitting
Fe40Al-2.5Ag	2	0.97	Pitting
	13	0.98	Pitting
	30	0.94	Pitting

Table 2 also shows that the Ag-modified intermetallic alloy showed major susceptibility to pitting corrosion since the LI value of this ternary alloy was close to 1, as shown by the polarization curves in Figure 3. Since silver is known to be immiscible in the iron aluminide matrix, this behavior may be due to the pitting corrosion induced by the galvanic couple formed by Ag and the binary Fe40Al matrix. Table 2 shows that the binary aluminide exhibited mixed corrosion at 2 and 13 exposure days, however, the corrosion type changed from mixed to uniform after 30 days of immersion. Pitting corrosion is typically related to larger electrochemical events than uniform corrosion [39]; see the comparison among intensities of the current transients shown in Figures 4, 5 and 6.

Figure 8 shows the variation of corrosion rate (mpy) as a function of immersion time for the binary Fe40Al and ternary Fe40Al-2.5Cr, Fe40Al-2.5Ag alloys exposed to Hank’s solution. The corrosion rate was determined based on the i_{corr} values obtained from the Stern-Geary equation, the Tafel slopes (from polarization curves), and the assumption that R_n is equivalent to R_p. This plot shows that Cr and Ag additions to the Fe40Al matrix decreased the corrosion rate, thus the Cr and Ag addition resulted in improved corrosion resistance. It is apparent that the Fe40Al-2.5Cr alloy displayed predominantly lower corrosion rates as compared with the Ag-modified intermetallic. However, the Fe40Al-2.5Cr corrosion rate tended to increase over the 30 day course of exposure, while the ternary Fe40Al-2.5Ag alloy tended to decrease over the entire period of exposure in Hank’s solution. This behavior may be associated with the more efficient protection of the Cr-modified Al-oxide film that formed on the Fe40Al-2.5Cr alloy.

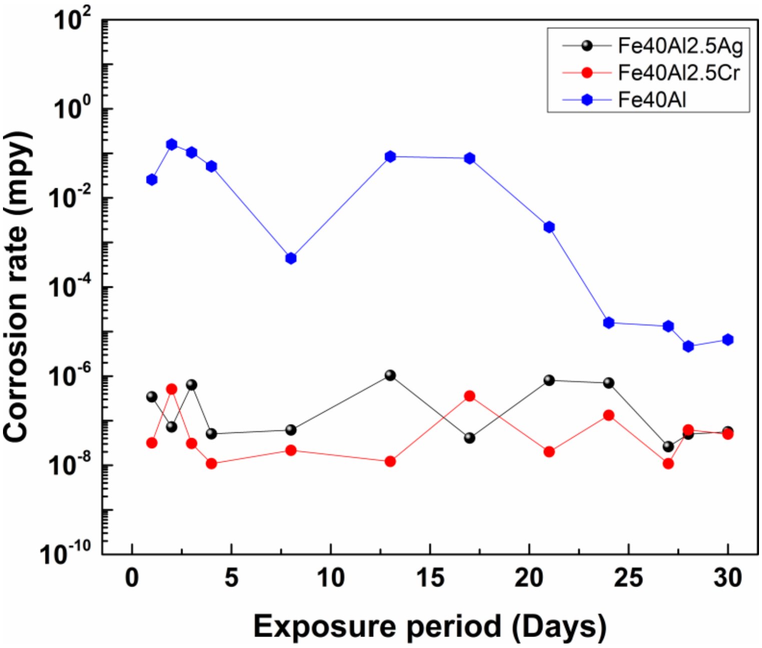

Figure 8. Corrosion rate as a function of exposure time for binary and ternary Fe40Al based alloys in Hank´s solution.

4. CONCLUSIONS

The corrosion behavior of Fe40Al based alloys in a simulated biological body environment was assessed to evaluate the potential of these materials for applications as metallic implants. The potentiodynamic polarization graphs revealed that Ag and Cr additions to binary Fe40Al promoted a passivation process in both ternary alloys, and Fe40Al-2.5Cr exhibited more pronounced passivation with subsequent pitting of the protective film. In accordance with electrochemical noise tests, both ternary intermetallic alloys underwent pitting corrosion over the entire exposure period; however, the binary Fe40Al alloy experienced mixed corrosion (uniform and pitting) over the 30 days of immersion. Assuming that R_n is equivalent to R_p, the addition of both Ag and Cr resulted in lower corrosion rates in both ternary alloys compared to the base binary alloy. Further, the Fe40Al-2.5Cr alloy exhibited the lowest corrosion rate over 30 days in contact with the synthetic biological solution. This behavior may be due to the Cr modification of the Al oxide film, which enhanced the protective nature of the surface film. In conclusion, Fe40Al based alloys can be utilized as biomaterials in contact with human body solutions, since these alloys exhibited good corrosion behavior.

ACKNOWLEDGMENTS
The authors of this work express their gratitude to the Physical Sciences Institute – UNAM as well as to the Research Center of Engineering and Applied Sciences - UAEMor for the use of its laboratories to develop the present project.

References

1. T. Matković, P. Matković and J. Malina, *J. Alloys Compd.*, 366 (1) (2004) 293.
2. J.A. Anderson, Appl. Dent. Materials, Blackwell Scientific Publications, sixth ed., (1985) Oxford.
3. S. Fujimoto, K. Tsujino, T. Shibata, *Electrochim. Acta*, 47(4) (2001) 543.
4. A.M. Bandar, R. Mongrain, E. Irissou, and S. Yue, *Surf. Coat. Technol.,* 216 (2013) 297.
5. R. A. Rodríguez-Díaz, A.L. Ramirez-Ledesma, M.A. Aguilar-Mendez, J.U. Chavarin, M.H. Gallegos and J.A. Juarez-Islas, *Int. J. Electrochem. Sci.*, 10 (2015) 2.
6. A.R.H. Bidhendi and M. Pouranvari, *Metalurgija*, 17(1) (2011) 13.
7. A. Balamurugan, S. Rajeswari, G. Balossier, A.H.S. Rebelo and J.M.F. Ferreira, *Mater. Corros.,* 59 (11) (2008) 855.
8. T. Hanawa, *Sci. Technol. Adv. Mater*., 3 (2002) 289.
9. E.P. Busso and F. A. McClintock, *Acta Metallurgica et Materialia,* 42(10) (1994) 3263.
10. R. Jayaram and M. K. Miller, *Acta Metallurgica et Materialia,* 42(5) (1994) 1561.
11. R.A. Rodríguez-Díaz, , M. Suárez, J. Juárez-Islas, M.G. Garnica-Romo, J. Arenas-Alatorre and J. Colín, *J. Appl. Res. Technol.,* 7(2) (2009) 233.
12. J. Porcayo-Calderon, R.A. Rodriguez-Diaz, E. Porcayo-Palafox, J. Colin, A. Molina-Ocampo and L. Martinez-Gomez, *Adv. Mater. Sci. Eng.,* 2015 (2015) 209286.
13. M.C. Garcia-Alonso, M.F. Lopez, M.L. Escudero, J.L. Gonzalez-Carrasco and D.G. Morris, *Intermetallics,* 7(2) (1999) 185.
14. M.F. Lopez, M.L. Escudero, E. Vida, A.R. Pierna and F.F. Marzo, *Electrochim. Acta,* 42 (1997) 659.
15. M.F. Lopez, A. Gutierrez, M.C. Alonso-Garcia and M.L. Escudero, *J. Mater. Res*., 13(1998) 314.
16. R.A. Rodriguez-Diaz, L. Banos, O, Novelo, C. Flores, J. Colin, J. Arenas-Alatorre and J.A. Juárez-Islas, *Acta Microsc.*, *18*(2) (2009) 169.
17. R. A. Rodríguez-Díaz, M. Suárez, J. Juárez-Islas, M. G. Garnica-Romo, J. Arenas-Alatorre and J. Colín, *J. Appl. Res. Technol.,* 7(2) (2009) 233.
18. D. Pavlyuchkov, B. Przepiórzyński, W. Kowalski, T.Y. Velikanova and B. Grushko, *Calphad*, 45 (2014) 194.
19. T.B. Massalski, Binary Alloy Phase Diagrams, 1 (1990) 35.
20. T.B. Massalski, Binary Alloy Phase Diagrams, 1 (1990) 8.
21. I.E.C. Robles, A.M. Villafañe, M.N. Flores, G. Gonzalez-Rodriguez and J.U. Chavarín, *ECS Trans.,* 29(1) (2010) 61.
22. N. Ohtsu, A. Nomura, M. Oku, T. Shishido and K. Wagatsuma, *Appl. Surf. Sci.,* 254(17) (2008) 5336.
23. C.D. Arrieta-Gonzalez, J. Porcayo-Calderon, V.M. Salinas-Bravo, J.G. Gonzalez-Rodriguez and J.G. Chacon-Nava, *Int. J. Electrochem. Sci.,* 6(9) (2011) 4016.
24. G.S. Frankel and N. Sridhar, *Mater. Chem. Phys.,* 104(1) (2007) 93.
25. M. Conradi, P.M. Schön, A. Kocijan, M. Jenko and G.J. Vancso, *Mater. Chem. Phys.*, 130(1-2) (2011) 708.
26. G.S. Frankel and N. Sridhar, *Mater. Today,* 11(10) (2008) 38.
27. P. Marcus, ed. *Corrosion mechanisms in theory and practice*. CRC press, 2011.
28. C. Gabrielli, and M. Keddam, *Corrosion,* 48(10) (1992) 794.
29. R.A. Cottis, *Corrosion,* 57(3) (2001) 265.
30. J.G. Llongueras, *Programa Universitario de Ciencia e Ingeniería de Materiales*, *UNAM, México,* (2002) 56.
31. H.A. A. Al-Mazeedi and R.A. Cottis, *Electrochim. Acta*, 49(17-18) (2004) 2787.
32. F. Mansfeld, Z. Sun and C.H. Hsu. *Electrochim. Acta,* 46(24-25) (2001) 3651.
33. S. Girija, U.K. Mudali, V.R. Raju, H.S. Khatak and B. Raj. *Mater. Sci. Eng., A,* 407(1-2) (2005) 188.

34. R.A. Cottis and S. Turgoose. *Mater. Sci. Forum*. Trans Tech Publications, 192 (1995) 663.
35. R.A. Cottis, M.A. Al-Ansari, G. Bagley and A. Pettiti, *Mater. Sci. Forum*. Trans Tech Publications. 289 (1998) 741.
36. G.S. Frankel, H.S Isaacs, J.R. Scully, J.D. Sinclair, *The Electrochemical Society*, *Proceeding Series NJ*, (2002) 430.
37. V. Freger and S. Bason, *J. Membr. Sci.*, 302(1-2) (2007) 1.
38. A.J. Bard, L.F. Faulkner, Electrochemical Methods, Wiley Interscience, 2000.
39. R. Cottis and S. Turgoose. *Electrochemical impedance and noise*. National Assn. of Corrosion Engineers. 7 (1999).